ACS APPLIED MATERIALS & INTERFACES

Research Article

www.acsami.org

One-Step Synthesis and Characterization of Polyaniline Nanofiber/Silver Nanoparticle Composite Networks as Antibacterial Agents

Selcuk Poyraz,[†] Idris Cerkez,[‡] Tung Shi Huang,[§] Zhen Liu,[†] Litao Kang,[∥] Jujie Luo,[∥] and Xinyu Zhang*[,†]

[†]Department of Polymer and Fiber Engineering, Auburn University, Auburn, Alabama 36849, United States

[‡]Department of Fiber and Polymer Engineering, Bursa Technical University, Bursa, 16190, Turkey

[§]Department of Poultry Science, Auburn University, Auburn, Alabama 36849, United States

[∥]College of Materials Science and Engineering, Taiyuan University of Technology, Taiyuan, Shanxi 030024, China

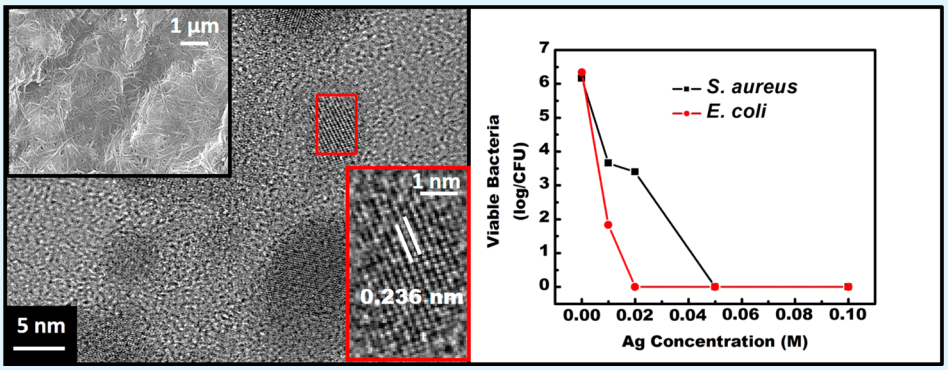

ABSTRACT: Through a facile and effective seeding polymerization reaction via a one-step redox/complexation process, which took place in aqueous medium at ambient temperature, silver nanoparticles (Ag NPs) embedded polyaniline nanofiber (PANI NF) networks were synthesized as antibacterial agents. During the reaction, not only NF morphology formation of the resulting conducting polymers (CPs) but also amplification of the aqueous silver nitrate ($AgNO_3$) solutions' oxidative potentials were managed by vanadium pentoxide (V_2O_5) sol–gel nanofibers, which acted as well-known nanofibrous seeding agents and the auxiliary oxidative agent at the same time. The PANI/Ag nanocomposites were proven to exhibit excellent antibacterial property against both Gram-negative *Escherichia coli* and Gram-positive *Staphylococcus aureus*. Antibacterial property performance and average life span of the nanocomposite network were optimized through the homogeneous distribution/embedment of Ag NPs within one-dimensional (1-D) PANI NF matrix. The antibacterial efficacy tests and nanocomposite material characterization results further indicated that the sole components of PANI/Ag have a synergistic effect to each other in terms of antibacterial property. Thus, this well-known catalytic seeding approach via a one-step oxidative polymerization reaction can be considered as a general methodology and a substantial fabrication tool to synthesize Ag NP decorated nanofibrillar PANI networks as advanced antibacterial agents.

KEYWORDS: *silver nanoparticle, polyaniline nanofiber, nanocomposite, antibacterial property*

INTRODUCTION

Throughout the last several decades (i) the emergence of various detrimental microorganisms[1] like bacterium, virus, mold, yeast, etc., and (ii) the increased possibility for humans to get exposed to these different strains in their daily living/working environments and to get more frequently infected by them[2] have been the major reasons behind all different studies with "antibacterial material" focus. Intensive research efforts have been devoted for such studies and their relevant applications in order to find substantial solutions that are targeting to ensure a cleaner/healthier life for people by effectively using these materials.[3] The diversity of the antibacterial materials used in such studies, including the renewable plant-based substances (tea extract,[2] chitosan[4−6]), noble/metal NPs, oxides and their cations (copper,[6,7] zinc,[6,7] titanium,[6,8] platinum,[9] Ag,[1,6−15] and gold[16]), CPs (PANI,[3,9,16−23] polyrhodanine,[24,25] polypyrrole[26]), *N*-halamines,[6,27−29] and carbon nanotubes,[30] etc., covers a very wide span. Among those materials, noble metal "Ag" has been the most sought after,[31] commonly engineered, and commercialized[13,14] by the researchers due to its distinguishing electrical, optical, long-term stable chemical, and catalytic properties.[6,8,32−34] In addition to its other uses in surface-enhanced Raman scattering (SERS),[8] photonic crystals,[35] catalysis,[14] nanoelectronic luminescent devices,[31] biochemical tagging,[35] food packaging,[13] sensory,[20] etc.,[34−39] Ag has particularly been known and utilized as a powerful antibacterial agent[2,36−40] in its elemental, NP, or cationic salt forms[6−8,10,11]

Received: August 20, 2014
Accepted: November 3, 2014
Published: November 3, 2014

 © 2014 American Chemical Society

Scheme 1. Illustration of the One-Step PANI/Ag Nanocomposite Synthesis

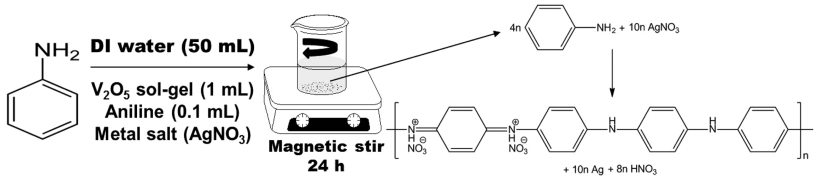

for the areas of curative and preventive health care[12,14,32,37] since ancient times.[2,11,36−40]

Owing to its above-mentioned properties and tremendous application potential in a wide variety of industrial fields, Ag has been considered as one of the major functionalizing agents[32,33] for the evergrowing polymer nanocomposites market.[8,31] Also, recent market forecasts indicate that global utilization of high value-added[40] composites made up of Ag has already exceeded million ton levels (>4) by the year 2011 with a promising annual growth rate of 24% and an expected demand worth of ∼$1 billion.[8,31,32] To properly address this increasing demand researchers from both academia and industry have agreed upon the implementation of "green" methods to synthesize Ag in its NP form.[8] These methods, which can be easily adapted to modern advancements in nanotechnology, aim to progressively relieve the cost pressure,[3] increase the efficiency of the as-synthesized material,[3] and more importantly maximize the use of environmentally benign solvents and nontoxic chemicals for the synthesis.[8] Thus, as an effort to minimize the impact of Ag on the environment[14] and to act accordingly with the above-mentioned goals of the green synthesis methods, Ag has been commonly used in its NP form while getting homogeneously dispersed/embedded inside polymeric matrices to form functionally advanced nanocomposites. In particular, their tunable morphologies and inherent long chains with relevant functional groups, which would act as targeted reactive sites and allow controllable immobilization of Ag NPs, are considered as the main reasons for choosing polymers as hosts.[8,32]

Another reason for the need of these composites synthesis is closely related to the toxicity of Ag^+ ions released from Ag NPs. On the basis of ongoing debates for a long while, many researchers believe that nano Ag and its cations are relatively safe for mammalian, plant, and other multicelled organisms' cells and their beneficial enzymes but it is hard to withdraw a commonly accepted conclusion from this topic.[14,32] Thus, synthesis of polymeric composites impregnated with Ag NPs has been offered as an advantageous solution to tackle this potential drawback[14] by hindering the release of Ag^+ ions to these cells' environment for a longer time[2] and restraining their direct uptake of Ag NPs.[32,39] In this manner, a great deal of research efforts have been spent on various studies, e.g., Jeon et al., Sotiriou et al., and Gu et al. prepared the long-time chemically durable silica/Ag nanocomposites,[2,14,35] Dowling et al. used polyurethane,[36] Shi et al. used poly(tetrafluoroethylene),[38] Kong et al. used poly(methyl methacrylate),[37] Wang et al. used polydopamine/poly(sulfobetaine methacrylate-*co*-acrylamide),[39] and Xue et al. used super hydrophobic cellulose fibers[40] where Nair et al. preferred to use methoxybenzyl chloride[31] as the host polymer to obtain their composites in a gram scale.

Among CPs family, PANI has been the most extensively studied one with respect to its many advantages such as easy and straightforward preparation,[41−44] low cost and high polymerization yield,[43] unique electrochemical and optical properties,[34,43] relatively high conductivity,[41−44] long-term chemical, thermal, and environmental stability,[34,41−45] good processability,[45] and most importantly its reversible (acid/base) doping/dedoping pathways identified with its structural chain nitrogen.[23,45] Thus, all these factors have spurred the use of PANI to fabricate its above-mentioned nanocomposites with Ag through different polymerization reactions, which were majorly carried out either in acidic (acetic,[46] nitric,[43,44,47,48] formic,[49] hydrochloric,[45] methane sulfonic,[50] and sulfuric[34]), ionic liquid,[41] organic solvent,[51] or aqueous[42,52] media. As for the synthesis, the in situ redox reaction between two nonconducting chemicals,[46,49] namely, aniline and $AgNO_3$, has been widely used as an efficient method to obtain nanocomposites made up of highly conducting PANI and Ag NPs[48−50] in the simplest manner and with syncretistic advantages.[43,46] The key to success for such reactions is "building substantial binding between nanocomposite compounds via their simultaneous formation". However, this opportunity remains as the biggest challenge of the in situ method, since compounds' size and morphology must be handled appropriately during the synthesis reaction.

Throughout the past decade nanostructured PANI, with different morphologies from 0-D nanoparticles to 3-D sea urchin-like nanospheres, has been copiously synthesized. Compared to all others 1-D nanostructured PANI, i.e., nanotubes (NTs)[42,48] and NFs,[45,52−56] has attracted intense attention due to their distinctive advantages for antibacterial applications. NTs have been observed to easily penetrate the bacteria cell wall like a syringe and form artificial pores and cause cell lysis,[25,26] whereas NFs offer a vast, highly porous scaffold which is more favorable for both expedited immobilization of Ag NPs and more bacteria cells attachment.[24,45] Upon further consideration of the fact about their synergistic[23] and complementary behavior to each other,[3,9,16,20] in terms of antibacterial property, PANI NF/Ag NP composites are expected to exhibit superior performance than those of their sole components through a host/guest interaction without any compromise.

Motivation of the current study was to develop a simple, efficient, affordable, and environmentally friendly method for synthesis of PANI/Ag nanocomposites as advanced antibacterial agents. To do that $AgNO_3$ was used as the oxidative and doping agent for aniline to get polymerized through a one-step redox reaction that took place in aqueous medium at ambient temperature. PANI NFs were generated under the guidance of nanofibrous V_2O_5 seeding agents, which were also contributing to the reaction as an auxiliary oxidative agent, while Ag NPs were simultaneously formed and immobilized within 1-D NFs matrix after getting reduced by them. Here, DI water was specifically selected as a "green" solvent in favor of both NF morphology formation and previously mentioned goals of the green synthesis methods to obtain intimately connected and uniform PANI/Ag nanocomposites.

MATERIALS AND METHODS

Materials. $AgNO_3$, aniline, and ammonium peroxydisulfate (APS) were all purchased from Alfa Aesar and used as received. Other reagents including potassium nitrate (KNO_3) and acetone (J. T. Baker) were of analytical grade and used without further purification. V_2O_5 sol–gel NF was prepared based on a previously reported method (Bailey et al. *J. Mater. Res.* **1992**, 7, 2530) using ammonium metavanadate (NH_4VO_3, Acros Organics) and Dowex Marathon (H) ion-exchange resin (Sigma-Aldrich) in DI water. Bacteria cultures of *S. aureus* (ATCC 6538) and *E. coli* (ATCC 43895) were purchased from American Type Culture Collection (Rockville, MD), and Trypticase soy agar was obtained from Difco Laboratories (Detroit, MI).

One-Step Synthesis of PANI NF/Ag NP Composite Networks (Scheme 1). In a typical experiment, 1 mL of V_2O_5 sol–gel NF was gently introduced into 50 mL of prestabilized DI water under magnetic stirring and its color changed to orange. After 10 min of magnetic stirring at ambient conditions, 0.1 mL of aniline monomer was added into this medium. Upon preliminary oxidative interactions between monomers and V_2O_5, starting from the first half of the following 10 min stirring, well-dispersed fibrous structures were being formed while changing the medium color to greenish yellow. Eventually, to obtain differently concentrated solutions of $AgNO_3$ (from 0.005 to 0.1 M) and to initiate the oxidative polymerization reactions, the required amount of metal salt was weighed and added into each system.

Since the synthesis reaction was conducted in aqueous medium and low-concentration $AgNO_3$ solutions ($\leq$0.02 M) there was a little lack of oxidative potential to polymerize all aniline monomers in the reaction medium; solution colors became greyish transparent instead of dark, indicating partial formation/dispersion of fibrous PANI precipitates. Thus, to compensate for this oxidative potential difference, a catalytic amount (0.057 g) of APS was finally added into these systems after 10 min of extra stirring, and this caused the expected darkening in reaction media colors.

A further reaction time of 24 h was given to all systems in order to obtain PANI NFs decorated with Ag NPs. At the end, resulting precipitates were suction filtered while getting washed with copious amounts of DI water and acetone. The damp precipitates were allowed to dry overnight in a vacuum oven at 80 °C. The yield of nanocomposite powders from different systems was ranging between 45 and 90 mg, since the Ag NP loading was determined by initial $AgNO_3$ concentration.[23,57]

Open-Circuit Potential Measurement of the Synthesis Reactions. OCP measurements were conducted on a CHI-601 D electrochemical workstation equipped with a conventional three-electrode cell system. The three electrodes, composed of platinum (Pt) gauze as the working electrode (WE), Pt wire as the counter electrode (CE), and Ag/AgCl as the reference electrode (RE), were immersed into the reaction medium. Before taking the measurements and adding reactants, 0.01 M KNO_3 was added into 50 mL of DI water under magnetic stirring in order to decay and stabilize the reaction potential at a steady state that took at most 20 min. The open-circuit condition was applied to the electrode cell system, while no current was passing through, and the potential difference between the WE and the RE was monitored continuously. A standard synthesis process (above explained) was performed, and its overall potential was monitored simultaneously as a function of time.

Characterization of PANI/Ag Nanocomposites. Different characterization techniques were used systematically to identify PANI/Ag nanocomposite networks. The overall morphology and composition of PANI/Ag were analyzed by a JEOL JSM-7000F scanning electron microscope (SEM) equipped with an energy-dispersive X-ray (EDX) detector. In-depth morphological analysis of PANI/Ag and crystalline nature determination of the Ag NPs were performed on a JEOL 2100F high-resolution transmission electron microscope (HR-TEM) operated at 200 kV and on a selected area electron diffractometer (SAED), respectively. The UV–visible light absorbance spectrum of PANI/Ag was obtained from a SHIMADZU UV-2450 spectrophotometer. Identification of the characteristic functional groups in PANI/Ag was done via Fourier transform infrared (FTIR) analysis, conducted on a Thermo Nicolet 6700 instrument. The thermal stability, solid residual, and Ag content of each PANI/Ag were all determined by thermal gravimetric analysis (TGA) performed on a TA Q2000 system. The optical nature of crystalline Ag nanoparticles formed during the synthesis reactions was explained by X-ray diffractometry (XRD) analysis, which was performed on a Rigaku powder X-ray diffractometer.

Electrical Conductivity Measurements with PANI/Ag Nanocomposites. The bulk electrical conductivity of the nanocomposites from different concentration systems was measured based on a linear four-probe method described elsewhere (Haupt et al. *J. Phys. Chem.* **1993**, 97, 7796). For the measurements, rectangular PANI/Ag thin films were obtained after they were applied 3500 psi pressure to fill a mold cavity with certain dimensions ($L \times W \times H$ = 1.5 cm × 0.2 cm × 0.225 cm), and then the four probe, connected to Agilent Technologies 34980A multifunctional switch/measure unit, was touched on thin film surfaces to read their resistivity values. Since the conductivity (σ = S/cm) is the reciprocal of electrical resistivity (R = Ω) it can be calculated with the equation $\sigma = L/(R \times A)$, where L represents the distance (0.52 cm) between the two inner probes and A represents the cross-sectional area of each nanocomposite film.

Antibacterial Efficacy Tests with PANI/Ag Nanocomposites. The antibacterial efficacy of PANI/Ag was evaluated against both Gram-positive *S. aureus* and Gram-negative *E. coli* through the dynamic flask shaking and sandwich tests.

Dynamic Flask Shaking Test. In a typical procedure, 10 mg of PANI/Ag was placed in sterilized 3 mL test tubes and then inoculated with 1 mL of a known population of bacteria suspension. Test tubes were rotated using a Mini LabRoller Rotator for specified contact times of 15, 30, 60, and 120 min, and then the bacterial solutions were serially diluted using 100 mM phosphate buffer solution (PBS) at pH 7 and placed on Trypticase soy agar plates. Bacterial colonies were enumerated after incubation at 37 °C for 24 h. The same procedure, without the presence of PANI/Ag, was followed as the control.

Sandwich Test. One inch by one inch filter paper swatches with ~15.5 wt % PANI/Ag sample on them were used for this test. Briefly, bacteria were suspended in 100 mM PBS (pH 7) buffer to specified populations. Next, an aliquot of 25 μL of bacterial suspension was placed on a swatch, and then an identical swatch was placed on top of it. In order to ensure adequate contact with bacteria, a sterile weight was applied on top of this sandwich. After 15, 30, 60, and 120 min contact times, the whole sandwich was placed in sterile tornado tubes containing 5 mL of 0.02 N sodium thiosulfate ($Na_2S_2O_3$) solution and vortexed for 2 min so that viable bacteria would be transferred from swatch surfaces to the solution. Eventually, serial dilutions were prepared using 100 mM PBS at pH 7 and placed on Trypticase soy agar plates. After incubation at 37 °C for 24 h, the bacterial colonies were recorded for analysis. The same procedure was followed for the uncoated filter papers, which served as control samples.

RESULTS AND DISCUSSION

Scheme 1 shows the one-step synthesis of PANI/Ag nanocomposites. A plausible formation mechanism is also proposed along with the results obtained from the OCP measurements in Figure 1. In situ monitoring of oxidative potential vs time profiles for two nanocomposite synthesis procedures, with and without APS, clearly revealed the dual role of V_2O_5 NFs both as seeding agents and as auxiliary oxidative agent. In contrast to the above-mentioned common synthesis reactions conducted in acidic media, the current "green" synthesis was carried out in DI water since it is an environmentally friendly, neutral solvent favorable for nanofibrous PANI synthesis.[48] However, the oxidative potential of just $AgNO_3$ was not enough to initiate an aqueous polymerization reaction at room temperature in a timely manner.[41] Thus, addition of a catalytic amount of V_2O_5 NF seeds in the reaction media (i) enhanced the overall oxidative potentials of both systems beyond 0.5 V, (ii) coordinately helped $AgNO_3$ to exceed the oxidation threshold

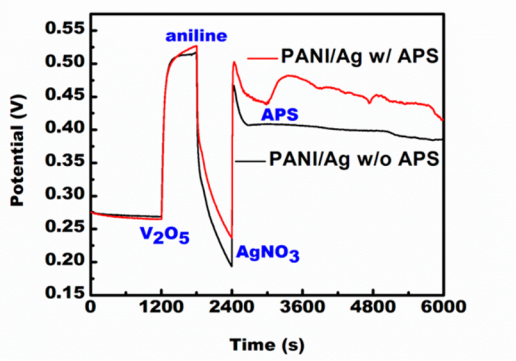

Figure 1. OCP patterns of the aqueous PANI/Ag synthesis reactions with and without APS.

of aniline via preoxidizing monomers at its surface, and (iii) provided rapid reaction kinetics for synthesis of PANI/Ag (less than 2 h the reaction potential reached steady state). Meanwhile, the as-synthesized PANI exhibited bulk NF morphology due to the seeding effect of V_2O_5 NFs, through which their morphology was duplicated by monomers and nanofibrous PANI oligomers were formed as reactive seeds, which would further promote bulk NFs formation.[57]

Morphological features of the as-synthesized PANI/Ag nanocomposites were verified by SEM and HR-TEM characterization. Figure 2A shows the homogeneously embedded/dispersed Ag NP clusters with 400−450 nm average diameters in 1-D PANI NF matrix. The same SEM image also shows the highly dense, straight, and micrometer long PANI NF network with narrow pores in it. The bright, prominent spots observed in this image, with ∼500 nm average diameters, indicate the embedded Ag NP clusters with high electron densities inside PANI NF matrix. EDX analysis of these spots and the more fibrous phase (Figure 3) proved that they were composed of elemental Ag and PANI NFs, respectively (Table 1). Like other noble metal NP systems, Ag NPs also tended to form clusters during the synthesis reactions due to their high surface energies, but they still kept their "particle" shapes on those clusters simply because of their electrochemical interactions with PANI NFs. Furthermore, similarly formed NP clusters were expected to exhibit distinctive size-dependent properties owing to their NPs' narrow particle size distribution (PSD) and facet compositions. On the other hand, PANI NF network was composed of 30−40 nm average diameter fibers and had very tight nanopores formed among its NF interspaces (Figure 2B).

Further characterization of PANI/Ag by HR-TEM provided more detailed information about its morphological properties. Similar to the SEM results, Ag NPs with average diameters from 5 to 65 nm could be seen as homogeneously decorating the PANI NFs web-like network composed of ∼35 nm thick fibers (Figure 2C). The SAED patterns (Figure 2C, inset) of Ag NPs indicate that they were perfect crystals, which were composed of small oxidized NPs with a PSD majorly (>75%) less than 10 nm (Figure 4). Additionally, the 0.236 nm average lattice fringe spacing of individual Ag NPs in Figure 2D (inset) was in good accordance with the previous literature,[23,31] indicating the presence of discrete (111) crystalline domains inside them. Here, the discrepancy between the sizes of Ag NPs in SEM and the HR-TEM images could be attributed to the sonication process that was applied for sample preparation purposes. The primary effects and advantages of these obvious morphological features on the antibacterial property of PANI/Ag will be explained in detail in the following sections.

After confirming the morphological features of PANI/Ag using SEM and TEM instruments, their further characterization including thermal, spectroscopic, crystallographic, and optical analyses were completed using relevant techniques. First, PANI NF and PANI/Ag nanocomposites were heated from room temperature up to 800 °C (at a heating rate of 10 °C/min in O_2 atmosphere) to determine the solid residue amount and the thermal stability of these samples. Figure 5A and its inset show

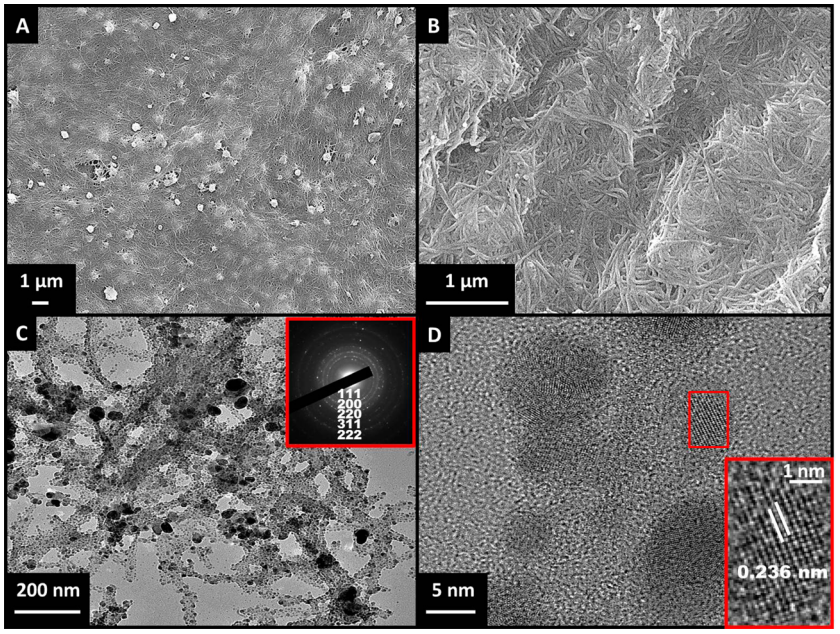

Figure 2. SEM images of (A) PANI/Ag nanocomposite showing homogeneously dispersed/embedded Ag NPs within PANI NF matrix, (B) zoomed-in fibrous PANI phase, (C) TEM image of PANI/Ag nanocomposite (inset, SAED pattern of Ag NPs), and (D) HR-TEM image of individual Ag NPs embedded into PANI NF matrix (inset, zoomed-in view of crystal lattice spacing in a single Ag NP).

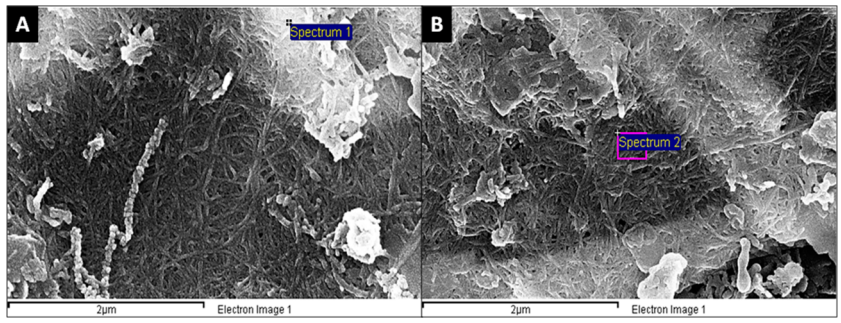

Figure 3. SEM images of (A) a bright spot indicating embedded Ag NP presence in PANI NF matrix and (B) nanofibrous PANI phase decorated with Ag NPs.

Table 1. Summary of the EDX Analysis Results from Figure 3

	C	Ag	Au	total
bright spot (at. %)		92.17	7.83	100
bright spot (wt %)		86.57	13.43	100
fibrous phase (at. %)	69.64	30.36		100
fibrous phase (wt %)	20.34	79.66		100

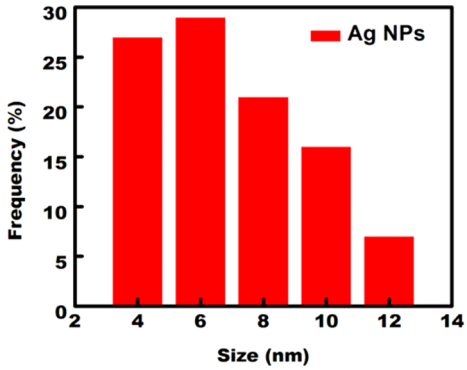

Figure 4. PSD analysis graphic of Ag NPs decorating the PANI NF network.

the TGA graphics obtained from these heating processes, according to which there were three main temperature regions that nanocomposite samples went through major weight losses. The first major weight loss, observed up to 100 °C, was corresponding to loss of water molecules/moisture that existed in the samples.[44,47] The secondary weight loss, observed up to 275 °C, could be attributed to volatilization and loss of nitrate (NO_3^-) dopants,[41,44,47] low molecular weight oligomers, and unreacted substances that were attached to the primary PANI chains.[3,9,20] The third major weight loss, observed between 300 and 450 °C, took place due to oxidative decomposition of the primary PANI NF backbone in each nanocomposite sample.[20,41] The extra weight loss occurring around 550 °C was probably due to decomposition of complex structures that were formed at the initial stages of the synthesis reactions at the interface of PANI NFs and Ag NPs.[57] The TGA results could be summarized as follows: (i) compared to bare PANI NFs both the thermal stability and the solid residue content of PANI/Ag samples were increased with the initial $AgNO_3$ concentration,[3] (ii) Ag NP loading in PANI/Ag samples was found to be around 57−77 wt %,[41,47] and (iii) the presence of PANI oligomers and polymeric PANI with different decomposition temperatures were observed in all samples due to the reasons listed in the nanocomposite synthesis section.[44,47] Lastly, the complexation process that took place between Ag NPs and amine/imine groups in PANI NFs reduced the as-formed PANI chains' mobility and caused a suppressive effect on chain transfer reactions, which positively contributed to the nanocomposites' thermal properties.[45]

FT-IR was used to investigate both pristine PANI NFs and stock PANI/Ag nanocomposite (Figure 5B). This characterization was applied to gain more insight about the formation of these nanostructures[42] and to confirm the presence of doped PANI by locating its functional groups' corresponding peaks and comparing their intensities.[45] On the basis of PANI NF's spectrum, the two distinct peaks located before and after 3200 cm^{-1} could be assigned to the asymmetric and symmetric

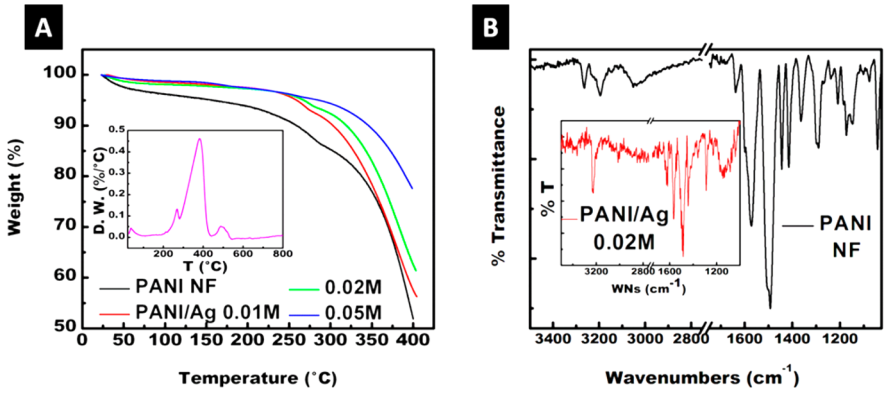

Figure 5. (A) TGA thermograms (inset, derived weight loss graphic) and (B) FT-IR spectra of PANI NF and PANI/Ag (inset, 0.02 M system's sample) nanocomposites.

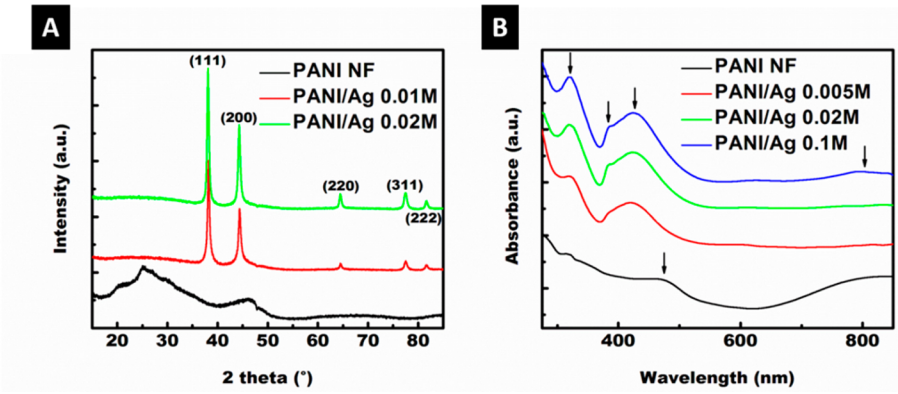

Figure 6. (A) XRD diffractograms and (B) UV−vis spectra of PANI NF and different PANI/Ag nanocomposites.

stretching modes of an aromatic amine (N−H) belonging to a $-NH_2$ group, respectively.[16,20,44] The following broad peak around 3050 cm^{-1} corresponded to a C−H stretching vibration.[9,20,41] A smaller peak, appearing around 1635 cm^{-1}, was characteristic of C═C stretching at quinoid (Q) and benzoid (B) emeraldine state PANI rings.[45] This peak was also assigned to the N−H scissoring vibration of an aromatic amine.[50] The two sharp peaks around 1570 and 1495 cm^{-1} corresponded to the stretching modes of N−Q−N and N−B−N groups of protonated PANI, respectively.[41−45,49,50] The two identical but less sharp peaks located at 1444 and 1415 cm^{-1} were related to the presence of oxidized and protonated aniline oligomers, respectively.[47,49] After these peaks the next one around 1360 cm^{-1} was assigned to stretching vibrations of an aromatic C−N group.[9,20] The following sharper peak around 1290 cm^{-1} indicated the stretching of the C−N group with secondary aromatic amine conjugation.[34,42,43] The next peak at 1200 cm^{-1} with a little hump around 1240 cm^{-1} was due to either the quinoic units in protonated PANI NF[16,44] or the stretching vibration of the $C-N^{(+\bullet)}$ group in polaron structure.[43,50] The following larger peak with two ends at 1170 and 1140 cm^{-1} was characteristic of the —N═Q—N^+—B— group in protonated PANI and stretching mode of C−N or in-plane C−H bonds, respectively.[41−43] Lastly, the peak around 1040 cm^{-1} corresponds to the stretching vibrations of the SO_3H^- group in APS-doped PANI NF.[20,41,50] The majority of the above listed characteristic PANI peaks, including the ones at 3200, 1635, 1570, 1495, 1444, and 1290 cm^{-1}, could be also observed in the PANI/Ag spectrum with some intensity loss and overlapping features (Figure 5B, inset). Most importantly, the peak around 1385 cm^{-1} proved the nitrate ($-NO_3$) counterion's presence in nanocomposites,[20,47−51] which were inserted in PANI NF backbones during the charge neutralization/doping process.

The crystalline nature of the as-obtained nanostructures was investigated by XRD analysis. Figure 6A shows the registered diffractograms of PANI NFs and PANI/Ag nanocomposites from 0.01 and 0.02 M systems, respectively. One broad and one sharper band on PANI NF's diffractogram, centered at 2θ = 20°,[3,9,16,20] and 25°,[34,41,42,45] were ascribed to the parallel and perpendicular periodicity of amorphous PANI chains. Another distinctive band observed around 2θ = 45° indicated the presence of local, partially crystalline PANI chains in NFs.[52,53,58] Such characteristic bands were broadened and diminished on PANI/Ag nanocomposite diffractograms due to the presence of highly crystalline Ag NPs in their structure. Here, the first two sharp and the latter three small peaks, located at 2θ = 38°, 44°, 64°, 77°, and 82°, represented Bragg's reflections from the (111), (200), (220), (311), and (222) planes of Ag NPs.[3,9,34,43−45,51] These results were in good accordance with the previously mentioned SAED pattern (Figure 2C, inset), the HR-TEM image (Figure 2D, inset), and the standard literature data, e.g., JCPDS No. 4-783,[20,35,39−42,52] which strongly indicate the existence of face-centered cubic (fcc) Ag NPs with dominant (111) lattice planes, immobilized in PANI NF matrix. Additionally, the effect of initial $AgNO_3$ concentration used for the nanocomposite synthesis on metal NPs' crystalline peak intensities could be obviously seen from these diffractograms as well.

The optical properties of PANI NFs and three different PANI/Ag nanocomposites from 0.005, 0.02, and 0.1 M concentrated systems were characterized by UV−vis spectroscopy. From the PANI NF spectrum in Figure 6B a tiny absorption peak located around 300−350 nm could be observed via the $\pi-\pi^*$ transition of benzoid rings in doped PANI chains.[9,16,44−47] The following broad shoulder at the same spectrum, located around 450−500 nm, was assigned to the polaron−π^* transition of the localized band and indicated the protonated/half-oxidized PANI structure for the NFs.[41,53,58] The last peak with a very broad free carrier tail, located around 800 nm, was ascribed to the π−polaron transition of emeraldine base PANI backbone.[3,20,34,42] Moreover, all three PANI/Ag nanocomposites' spectra in Figure 6B clearly exhibited the above-mentioned characteristic absorption peaks of PANI, especially at higher concentrations of $AgNO_3$. However, there was a high possibility of shifting in those peaks toward to the red region due to the oxidative interactions between PANI and $AgNO_3$, which took place along the nanocomposite synthesis.[9,41,45] During the in situ polymerization reaction, $AgNO_3$ was reduced by nitrogen at amine groups via transforming them into imines.[20] Also, the overlapping feature between the surface plasmon resonance (SPR) peak of embedded Ag NPs and the polaron band of PANI could be clearly observed from each PANI/Ag nanocomposite's spectrum.[3,34,42] The SPR peak appeared as a tiny shoulder on the polaron PANI band around 400 nm with increasing intensity proportional to the initial $AgNO_3$ concentration, just like the other characteristic PANI peaks on these spectra.[2,49−51]

Lastly, the bulk electrical conductivity (σ) of the PANI/Ag nanocomposite films was measured as previously explained by a four-probe method to determine its contribution to the antibacterial performance. The overall σ of the nanocomposites from different concentrated systems was in the range from 2 ×

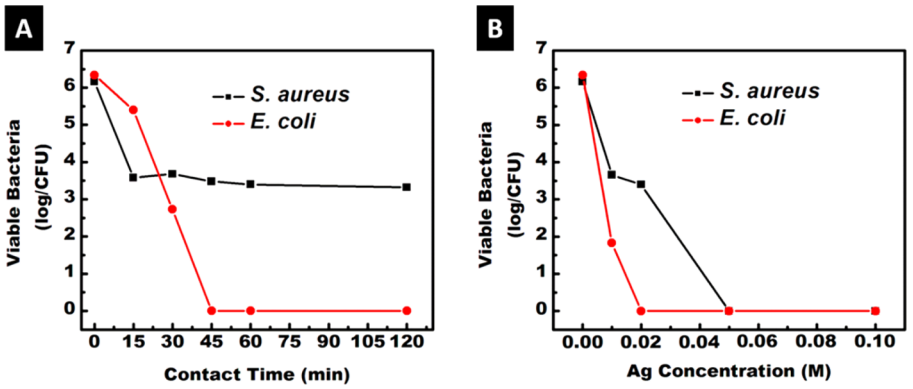

Figure 7. Antibacterial efficacy test results obtained from dynamic flask shaking (A) with PANI/Ag 0.02 M nanocomposite for different contact times and (B) with PANI/Ag from 0.01, 0.02, 0.05, and 0.1 M systems for 60 min contact time.

10^{-3} to 0.196 S/cm. The values were in good agreement with the synthesis method used. Since the reaction medium was DI water, PANI NFs in nanocomposites lacked acidic dopants, on which their electrical conductivity majorly depends. Other than that there was a linear relationship observed between the σ and the Ag concentration used for the synthesis. Thus, it would be reasonable to expect a better antibacterial performance for the nanocomposites obtained from higher concentrated systems.

Upon completion of the in-depth characterization of PANI NFs and PANI/Ag nanocomposites, the success of our one-step, oxidative seeding agent-assisted polymerization reaction was confirmed. Afterward, antibacterial efficacies of these nanostructures against Gram-positive and Gram-negative bacteria were further evaluated by dynamic flask shaking and sandwich tests. The results obtained from two different dynamic flask shaking tests are summarized in Figure 7 and Table 2. It can be seen that the control (empty filter paper)

Table 2. Summary of the Antibacterial Efficacy Results from Dynamic Flask Shaking Tests

		bacteria reduction (log/CFU)	
sample	contact time (min)	*S. aureus*	*E. coli*
filter paper	120	0.04	0.01
PANINF	120	0.16	0.05
PANI/Ag 0.02 M	15	2.58	0.94
	30	2.48	3.61
	45	2.68	6.34
	60	2.76	6.34
	120	2.84	6.34
PANI/Ag 0.01 M	60	2.50	4.51
PANI/Ag 0.02 M	60	2.76	6.34
PANI/Ag 0.05 M	60	6.16	6.34
PANI/Ag 0.10 M	60	6.16	6.34

sample did not exhibit any obvious reduction in viable bacteria even for the longest contact time, but since PANI is a known biocide,[17−19,23] the other control sample with just PANI NFs caused a very limited reduction (Table 2). On the other hand, introduction of Ag NPs into PANI NFs significantly enhanced the antibacterial efficacy of nanocomposites to both types of bacteria. Thus, PANI/Ag nanocomposites were evaluated in two different ways to determine the antibacterial effects of Ag NPs. First, stock PANI/Ag nanocomposite sample from the 0.02 M system was used against both bacteria strains during different contact times, i.e., 15, 30, 45, 60, and 120 min, in order to reveal the kinetic reduction effect. To analyze the effect of Ag concentration, in the second experiment, different PANI/Ag nanocomposites from 0.01, 0.02, 0.05, and 0.1 M systems were used against both bacteria strains for a constant contact time of 60 min. On the basis of the results shown in Figure 7A, a longer contact time increased the bacterial reduction.

Here, the reduction in *E. coli* was more obvious than that of *S. aureus*. Also, as expected, a higher Ag concentration in nanocomposite samples caused more inactivation in both strains (Figure 7B). This was a clear indication that Ag NPs are the predominant biocide in nanocomposite structures. Moreover, the PANI/Ag nanocomposite from the 0.05 M system succeeded in complete inactivation of both bacteria strains within 60 min contact time. Generally, for all different Ag concentrations, PANI/Ag nanocomposite seemed to be more effective on Gram-negative bacteria than it was on Gram-positive bacteria. For instance, the stock PANI/Ag nanocomposite was able to completely inactivate all *E. coli* bacteria within 45 min contact time, whereas it could only cause ∼2.7 log reductions on *S. aureus*. As previously observed in various studies, this result was clearly indicating the difference in resistance against Ag for these bacteria strains that originates from their peptidoglycan layouts. Thus, having a thicker peptidoglycan layer around its cell provides more protection to *S. aureus* and effectively prevented penetration of Ag NPs through its cell wall.[3,11,13,23,26,59]

More reliable antibacterial efficacy evaluations on surfaces were carried out through sandwich tests using the above-mentioned samples-coated filter papers. Since PANI/Ag 0.02 M nanocomposite sample provided sufficient inactivation for the dynamic flask shaking test, corresponding nanocomposite sample coated filter paper swatches were used for this test along with just PANI NF coated, and the uncoated filter papers served as controls. The as-obtained results from these tests are shown in Figure 8 and Table 3. As given in Table 3, empty filter paper provided about 0.53 and 0.28 log reductions against *S. aureus* and *E. coli*, respectively. This reduction was caused by either the adhesion and/or the physical entrapment of bacteria cells within the fibrous matrix of the filter paper. On the other hand, due to its above-mentioned biocide property, pristine PANI NF-coated swatches provided limited inactivation of 1.85 and ∼2.4 log reductions on each bacteria strain within 120 min contact time.

Similar to the dynamic flask shaking test results, PANI/Ag 0.02 M nanocomposite containing sandwiches provided

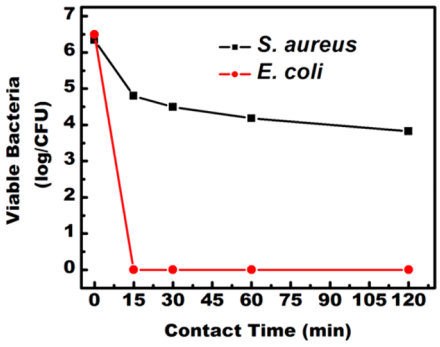

Figure 8. Antibacterial efficacy test results obtained from sandwich tests with PANI/Ag 0.02 M nanocomposites for 15, 30, 60, and 120 min contact times.

Table 3. Summary of the Antibacterial Efficacy Results from Sandwich Tests

		bacteria reduction (log reduction/CFU)	
sample	contact time (min)	*S. aureus*	*E. coli*
filter paper	120	0.53	0.28
PANI NF	120	1.85	2.39
PANI/Ag 0.02 M	15	1.54	6.50
	30	1.85	6.50
	60	2.16	6.50
	120	2.52	6.50

powerful antibacterial performance via complete inactivation of the Gram-negative bacteria cells and 1.54 log reduction on the viable Gram-positive bacteria within 15 min contact time. This result was most probably related to the increased exposure of *E. coli* cells to PANI/Ag nanocomposite in sandwich form. However, increasing contact times did not significantly improve the efficacies against *S. aureus* cells. Although it was not presented here, based on the dynamic flask shaking test results it was anticipated that using PANI/Ag nanocomposites from higher concentrated systems better efficacies against Gram-positive bacteria could be obtained.

The broad-spectrum antibacterial performances of PANI NF and different PANI/Ag nanocomposite samples were evaluated in detail via dynamic flask shaking and sandwich tests. It was proven that both samples were able to kill and/or inhibit the growth of medically hazardous Gram-positive and Gram-negative bacteria strains.[3,16−20] On the basis of these test results a plausible working mechanism about the antibacterial properties of PANI NFs and PANI/Ag nanocomposites is proposed and strongly supported with the information from the previous literature as follows. Compared to PANI/Ag nanocomposites, the pristine PANI NFs exhibited a limited antibacterial performance in both tests against *E. coli* and *S. aureus*, which was mainly related to its chemical nature.[19] Since they were synthesized in neutral medium, i.e., DI water, PANI NFs lacked acidic dopant molecules on their primary backbone chains, which are the main compounds that their antibacterial property depends on.[19,23]

Other than these molecules, a different polarity charge transfer process, which took place when PANI NFs and bacteria cells electrostatically adhered to each other, could be another important factor providing antibacterial property for PANI NFs.[18,19,23] Lastly, PANI NFs' higher antibacterial performance against *E. coli* could be ascribed to their multilayered Gram-negative cell walls with low osmotic pressure, which facilitated their physical interactions.[3] Additionally, the surface hydrophilicity, polymeric chain length, low molecular weight, and inherent amino groups' presence could be listed as other important factors[16] for PANI that (i) increased the overall permeability of bacteria cell membranes and (ii) exerted repressive effect on damage-responsive genes, which are primarily involved in energy metabolism and transport, cell wall repairment, and formation of stress-resistant biofilms, in order to mitigate potential chances of the emergence of bacterial resistance.[16,17]

As for the silver component's antibacterial working mechanism, chances were related to either (i) the size distribution and nature of its NPs or (ii) the release rate of its cations toward the bacteria medium and their possible physicochemical interactions with electron donor biological molecules containing S, O, N, or essential metal cations in bacteria cell walls such as Ca^{2+} or Zn^{+}.[6,12−15,32,36] On the basis of the PSD analysis results, >75% of the Ag NPs in PANI/Ag nanocomposites were found in the size range of 4−8 nm. Along with the previous literature, this data indicates a large amount of Ag^{+} release took place from Ag NPs surface to the bacteria environment, which would interfere with the metabolic pathways, i.e., ATP production and DNA replication,[32] of bacteria cells and provide the major antibacterial property for PANI/Ag nanocomposites.[13,14,23,26] Also, the penetration and binding strength of these NPs in bacteria cell membranes were observed to be higher, which is advantageous for their bactericidal effect that is based on chemically interacting with the S- and P-containing compounds, i.e., DNA or proteins,[1,8] and causing malfunctioning on them.[13] However, the rest (~25%) of Ag NPs (up to 12 nm particle size) were also effectively contributing to the antibacterial performance of PANI/Ag nanocomposites via getting attached to the bacteria cell membranes and disturbing their in-cell transport or respiratory functions.[8,13,14] In addition, on the readily oxidized and highly reactive (111) facet dominating surfaces of such NPs, large amounts of oxidative stress and reactive oxygen species were formed, and they disrupted the lipids, cytoplasm, and DNA of bacteria cells.[1,6,8,13,32] As repeatedly suggested in previous literature, to have better control of the NP morphology,[6] prolong the release of Ag^{+} cations from the NPs,[15,23,32,36] minimize the toxicity of Ag^{+} cations to prevent damaging multicelled organisms' cells and their beneficial enzymes,[6,14,23] obtain a synergistic effect on antibacterial property, and optimize its duration,[3,6,9,16] in this study Ag NPs were homogeneously embedded into PANI NFs network.

CONCLUSION

Along with the driving force of modern nanotechnology, in order to properly address the demand in the constantly expanding nanocomposite market with Ag NPs and to provide a promising solution for the continuously growing threat of the pathogenic microorganisms' emergence, in this study, PANI NF networks with homogeneous Ag NP decoration were facilely synthesized in a nanocomposite form. To the best of our knowledge, such nanocomposites were, for the first time, obtained through a one-step oxidative seeding template-assisted polymerization reaction, which took place in "green" DI water medium at room temperature and without the need of any harsh acids or oxidative agents.

According to the strongly supported material characterization results, the as-synthesized nanocomposites were found to

exhibit unique chemical and morphological features with substantial integrity between their counterparts, which turned out to be advantageous for their final use as powerful antibacterial agents. Besides, the four-probe conductivity measurement results along with the dynamic flask shaking and sandwich test results revealed the clear relationship between the promising antibacterial property of these nanocomposites against both Gram-positive and Gram-negative bacteria and the initial Ag concentration used for nancomposite synthesis. On the basis of the overall results and support from the previous literature, PANI/Ag nanocomposites were found to be more effective on Gram-negative *E. coli* than Gram-positive *S. aureus* due to the difference in their peptidoglycan layouts. Lastly, homogeneous embedment of Ag NPs into PANI NF networks was proven to have a synergistic and complementary effect on each individual's antibacterial performance, broadened the life span, minimized the cytotoxicity of Ag^+ cations on the other living organisms' cells, and enriched the dual antibacterial property duration of PANI/Ag nanocomposites.

We believe that the synthesis of such elaborately combined hybrid nanocomposites will help to elucidate the insights of their bactericidal working mechanisms and provide more active materials for next-generation antibacterial applications.

AUTHOR INFORMATION

Corresponding Author

*Tel.: 1-334-844-5439; fax: 1-334-844-4068; e-mail: xzz0004@auburn.edu.

Notes

The authors declare no competing financial interest.

ACKNOWLEDGMENTS

We gratefully acknowledge financial support from National Science Foundation Award CMMI-1000491 and Auburn University. We also thank Dr. Ning Lu and Dr. Moon J. Kim for their help with TEM imaging.

REFERENCES

(1) Morones, J. R.; Elechiguerra, J. L.; Camacho, A.; Holt, K.; Kouri, J. B.; Ramirez, J. T.; Yacaman, M. J. The Bactericidal Effect of Silver Nanoparticles. *Nanotechnology* **2005**, *16*, 2346−2353.

(2) Jeon, H. J.; Yi, S. C.; Oh, S. G. Preparation and Antibacterial Effects of Ag-SiO_2 Thin Films by sol-gel Method. *Biomaterials* **2003**, *24*, 4921−4928.

(3) Jia, Q. M.; Shan, S. Y.; Jiang, L. H.; Wang, Y. M.; Li, D. Synergistic Antimicrobial Effects of Polyaniline Combined with Silver Nanoparticles. *J. Appl. Polym. Sci.* **2012**, *125*, 3560−3566.

(4) Qin, C. Q.; Li, H. R.; Xiao, Q.; Liu, Y.; Zhu, J. C.; Du, Y. M. Water-solubility of Chitosan and its Antimicrobial Activity. *Carbohydr. Polym.* **2006**, *63*, 367−374.

(5) Rabea, E. I.; Badawy, M. E. T.; Stevens, C. V.; Smagghe, G.; Steurbaut, W. Chitosan as Antimicrobial Agent: Applications and Mode of Action. *Biomacromolecules* **2003**, *4*, 1457−1465.

(6) Simoncic, B.; Tomsic, B. Structures of Novel Antimicrobial Agents for Textiles-A Review. *Text. Res. J.* **2010**, *80*, 1721−1737.

(7) Kim, T. N.; Feng, Q. L.; Kim, J. O.; Wu, J.; Wang, H.; Chen, G. Q.; Cui, F. Z. Antimicrobial Effects of Metal Ions (Ag^+, Cu^{2+}, Zn^{2+}) in Hydroxyapatite. *J. Mater. Sci.-Mater. Med.* **1998**, *9*, 129−134.

(8) Sharma, V. K.; Yngard, R. A.; Lin, Y. Silver Nanoparticles: Green Synthesis and Their Antimicrobial Activities. *Adv. Colloid Interface Sci.* **2009**, *145*, 83−96.

(9) Boomi, P.; Prabu, H. G.; Mathiyarasu, J. Synthesis and Characterization of Polyaniline/Ag-Pt Nanocomposite for Improved Antibacterial Activity. *Colloids Surf., B* **2013**, *103*, 9−14.

(10) Clement, J. L.; Jarrett, P. S. Antibacterial Silver. *Met.-Based Drugs* **1994**, *1*, 467−482.

(11) Feng, Q. L.; Wu, J.; Chen, G. Q.; Cui, F. Z.; Kim, T. N.; Kim, J. O. A Mechanistic Study of the Antibacterial Effect of Silver Ions on Escherichia coli and Staphylococcus aureus. *J. Biomed. Mater. Res.* **2000**, *52*, 662−668.

(12) Schierholz, J. M.; Lucas, L. J.; Rump, A.; Pulverer, G. Efficacy of Silver-coated Medical Devices. *J. Hosp. Infect.* **1998**, *40*, 257−262.

(13) Sotiriou, G. A.; Pratsinis, S. E. Engineering Nanosilver as an Antibacterial, Biosensor and Bioimaging Material. *Curr. Opin. Chem. Eng.* **2011**, *1*, 3−10.

(14) Sotiriou, G. A.; Pratsinis, S. E. Antibacterial Activity of Nanosilver Ions and Particles. *Environ. Sci. Technol.* **2010**, *44*, 5649−5654.

(15) Xinping, L.; Shengli, L.; Miaotao, Z.; Chuanghong, L. Evaluations of Antibacterial Activity and Cytotoxicity on Ag Nanoparticles. *Rare Met. Mater. Eng.* **2011**, *40*, 0209−0214.

(16) Boomi, P.; Prabu, H. G. Synthesis, Characterization and Antibacterial Analysis of Polyaniline/Au-Pd Nanocomposite. *Colloids Surf., A* **2013**, *429*, 51−59.

(17) Gizdavic-Nikolaidis, M. R.; Bennett, J. R.; Swift, S.; Easteal, A. J.; Ambrose, M. Broad Spectrum Antimicrobial Activity of Functionalized Polyanilines. *Acta Biomater.* **2011**, *7*, 4204−4209.

(18) Seshadri, D. T.; Bhat, N. V. Use of Polyaniline as an Antimicrobial Agent in Textiles. *Indian J. Fibre Text.* **2005**, *30*, 204−206.

(19) Shi, N. L.; Guo, X. M.; Jing, H. M.; Gong, J.; Sun, C.; Yang, K. Antibacterial Effect of the Conducting Polyaniline. *J. Mater. Sci. Technol.* **2006**, *22*, 289−290.

(20) Tamboli, M. S.; Kulkarni, M. V.; Patil, R. H.; Gade, W. N.; Navale, S. C.; Kale, B. B. Nanowires of Silver-Polyaniline Nanocomposite Synthesized via in situ Polymerization and its Novel Functionality as an Antibacterial Agent. *Colloids Surf., B* **2012**, *92*, 35−41.

(21) Kucekova, Z.; Kasparkova, V.; Humpolicek, P.; Sevcikova, P.; Stejskal, J. Antibacterial Properties of Polyaniline-Silver Films. *Chem. Pap.* **2013**, *67*, 1103−1108.

(22) Chauhan, N. P. S.; Ameta, R.; Ameta, R.; Ameta, S. C. Biological Activity of Emeraldine Bases of Polyaniline. *J. Indian Chem. Counc.* **2010**, *27*, 128−133.

(23) Agarwala, M.; Barman, T.; Gogoi, D.; Choudhury, B.; Pal, A. R.; Yadav, R. N. S. Highly Effective Antibiofilm Coating of Silver−Polymer Nanocomposite on Polymeric Medical Devices Deposited by One step Plasma Process. *J. Biomed. Mater. Res., Part B* **2014**, *102B*, 1223−1235.

(24) Kong, H.; Jang, J. Synthesis and Antimicrobial Properties of Novel Silver/Polyrhodanine Nanofibers. *Biomacromolecules* **2008**, *9*, 2677−2681.

(25) Kong, H.; Song, J.; Jang, J. One-step Preparation of Antimicrobial Polyrhodanine Nanotubes with Silver Nanoparticles. *Macromol. Rapid Commun.* **2009**, *30*, 1350−1355.

(26) Park, E.; Kim, H.; Song, J.; Oh, H.; Song, H.; Jang, J. Synthesis of Silver Nanoparticles Decorated Polypyrrole Nanotubes for Antimicrobial Application. *Macromol. Res.* **2012**, *20*, 1096−1101.

(27) Cerkez, I.; Kocer, H. B.; Worley, S. D.; Broughton, R. M.; Huang, T. S. N-Halamine Biocidal Coatings via a Layer-by-Layer Assembly Technique. *Langmuir* **2011**, *27*, 4091−4097.

(28) Kocer, H. B.; Cerkez, I.; Worley, S. D.; Broughton, R. M.; Huang, T. S. Polymeric Antimicrobial N-Halamine Epoxides. *ACS Appl. Mater. Interfaces* **2011**, *3*, 2845−2850.

(29) Kocer, H. B.; Cerkez, I.; Worley, S. D.; Broughton, R. M.; Huang, T. S. N-Halamine Copolymers for Use in Antimicrobial Paints. *ACS Appl. Mater. Interfaces* **2011**, *3*, 3189−3194.

(30) Kang, S.; Pinault, M.; Pfefferle, L. D.; Elimelech, M. Single-Walled Carbon Nanotubes Exhibit Strong Antimicrobial Activity. *Langmuir* **2007**, *23*, 8670−8673.

(31) Nair, A. S.; Binoy, N. P.; Ramakrishna, S.; Kurup, T. R. R.; Chan, L. W.; Goh, C. H.; Islam, M. R.; Utschig, T.; Pradeep, T. Organic-Soluble Antimicrobial Silver Nanoparticle-Polymer Compo-

sites in Gram Scale by One-Pot Synthesis. *ACS Appl. Mater. Interfaces* **2009**, *1*, 2413−2419.
(32) Dallas, P.; Sharma, V. K.; Zboril, R. Silver Polymeric Nanocomposites as Advanced Antimicrobial Agents: Classification, Synthetic Paths, Applications, and Perspectives. *Adv. Colloid Interface Sci.* **2011**, *166*, 119−135.
(33) Wei, Q. F.; Ye, H.; Hou, D. Y.; Wang, H. B.; Gao, W. D. Surface Functionalization of Polymer Nanofibers by Silver Sputter Coating. *J. Appl. Polym. Sci.* **2006**, *99*, 2384−2388.
(34) Drury, A.; Chaure, S.; Kroell, M.; Nicolosi, V.; Chaure, N.; Blau, W. J. Fabrication and Characterization of Silver/Polyaniline Composite Nanowires in Porous Anodic Alumina. *Chem. Mater.* **2007**, *19*, 4252−4258.
(35) Gu, G. X.; Xu, J. X.; Wu, Y. F.; Chen, M.; Wu, L. M. Synthesis and Antibacterial Property of Hollow SiO_2/Ag Nanocomposite Spheres. *J. Colloid Interface Sci.* **2011**, *359*, 327−333.
(36) Dowling, D. P.; Donnelly, K.; McConnell, M. L.; Eloy, R.; Arnaud, M. P. Deposition of Anti-bacterial Silver Coatings on Polymeric Substrates. *Thin Solid Films* **2001**, *398*, 602−606.
(37) Kong, H.; Jang, J. Antibacterial Properties of Novel Poly(methyl methacrylate) Nanofiber Containing Silver Nanoparticles. *Langmuir* **2008**, *24*, 2051−2056.
(38) Shi, Z. Q.; Zhou, H.; Qing, X. T.; Dai, T. Y.; Lu, Y. Facile Fabrication and Characterization of Poly(tetrafluoroethylene)@ Polypyrrole/Nano-silver Composite Membranes with Conducting and Antibacterial Property. *Appl. Surf. Sci.* **2012**, *258*, 6359−6365.
(39) Wang, R.; Neoh, K. G.; Kang, E.-T.; Tambyah, P. A.; Chiong, E. Antifouling Coating with Controllable and Sustained Silver Release for Long-term Inhibition of Infection and Encrustation in Urinary Catheters. *J. Biomed. Mater. Res., Part B* **2014**, in press.
(40) Xue, C. H.; Chen, J.; Yin, W.; Jia, S. T.; Ma, J. Z. Superhydrophobic Conductive Textiles with Antibacterial Property by Coating Fibers with Silver Nanoparticles. *Appl. Surf. Sci.* **2012**, *258*, 2468−2472.
(41) Correa, C. M.; Faez, R.; Bizeto, M. A.; Camilo, F. F. One-pot Synthesis of a Polyaniline-Silver Nanocomposite Prepared in Ionic Liquid. *RSC Adv.* **2012**, *2*, 3088−3093.
(42) Gao, Y.; Shan, D. C.; Cao, F.; Gong, J.; Li, X.; Ma, H. Y.; Su, Z. M.; Qu, L. Y. Silver/Polyaniline Composite Nanotubes: One-step Synthesis and Electrocatalytic Activity for Neurotransmitter Dopamine. *J. Phys. Chem. C* **2009**, *113*, 15175−15181.
(43) Reda, S. M.; Al-Ghannam, S. M. Synthesis and Electrical Properties of Polyaniline Composite with Silver Nanoparticles. *Adv. Mater. Phys. Chem.* **2012**, *2*, 75−81.
(44) Wankhede, Y. B.; Kondawar, S. B.; Thakare, S. R.; More, P. S. Synthesis and Characterization of Silver Nanoparticles Embedded in Polyaniline Nanocomposite. *Adv. Mater. Lett.* **2013**, *4*, 89−93.
(45) Grinou, A.; Bak, H.; Yun, Y. S.; Jin, H. J. Polyaniline/Silver Nanoparticle-Doped Multiwalled Carbon Nanotube Composites. *J. Dispersion Sci. Technol.* **2012**, *33*, 750−755.
(46) Blinova, N. V.; Bober, P.; Hromadkova, J.; Trchova, M.; Stejskal, J.; Prokes, J. Polyaniline-Silver Nanocomposites Prepared by the Oxidation of Aniline with Silver Nitrate in Acetic Acid Solutions. *Polym. Int.* **2010**, *59*, 437−446.
(47) Blinova, N. V.; Stejskal, J.; Trchova, M.; Sapurina, I.; Ciric-Marjanovic, G. The Oxidation of Aniline with Silver Nitrate to Polyaniline-Silver Composites. *Polymer* **2009**, *50*, 50−56.
(48) Stejskal, J.; Prokes, J.; Sapurina, I. The Reduction of Silver Ions with Polyaniline: The Effect of the Type of Polyaniline and the Mole Ratio of the Agents. *Mater. Lett.* **2009**, *63*, 709−711.
(49) Bober, P.; Stejskal, J.; Trchova, M.; Hromadkova, J.; Prokes, J. Polyaniline-Coated Silver Nanowires. *React. Funct. Polym.* **2010**, *70*, 656−662.
(50) Bober, P.; Stejskal, J.; Trchova, M.; Prokes, J. Polyaniline-Silver Composites Prepared by the Oxidation of Aniline with Mixed Oxidants, Silver Nitrate and Ammonium Peroxydisulfate: The Control of Silver Content. *Polymer* **2011**, *52*, 5947−5952.
(51) Paulraj, P.; Janaki, N.; Sandhya, S.; Pandian, K. Single Pot Synthesis of Polyaniline Protected Silver Nanoparticles by Interfacial Polymerization and Study its Application on Electrochemical Oxidation of Hydrazine. *Colloids Surf., A* **2011**, *377*, 28−34.
(52) Gao, L.; Lv, S.; Xing, S. X. Facile Route to Achieve Silver@ Polyaniline Nanofibers. *Synth. Met.* **2012**, *162*, 948−952.
(53) Chiou, N. R.; Epstein, A. J. Polyaniline Nanofibers Prepared by Dilute Polymerization. *Adv. Mater.* **2005**, *17*, 1679−1683.
(54) Huang, J. X.; Kaner, R. B. Nanofiber Formation in the Chemical Polymerization of Aniline: A Mechanistic Study. *Angew. Chem., Int. Ed.* **2004**, *43*, 5817−5821.
(55) Surwade, S. P.; Manohar, N.; Manohar, S. K. Origin of Bulk Nanoscale Morphology in Conducting Polymers. *Macromolecules* **2009**, *42*, 1792−1795.
(56) Zhang, X. Y.; Kolla, H. S.; Wang, X. H.; Raja, K.; Manohar, S. K. Fibrillar Growth in Polyaniline. *Adv. Funct. Mater.* **2006**, *16*, 1145−1152.
(57) Liu, Z.; Liu, Y.; Zhang, L.; Poyraz, S.; Lu, N.; Kim, M.; Smith, J.; Wang, X. L.; Yu, Y. J.; Zhang, X. Y. Controlled Synthesis of Transition Metal/Conducting Polymer Nanocomposites. *Nanotechnology* **2012**, *23*, 335603.
(58) Kan, J. Q.; Zhang, S. L.; Jing, G. L. Effect of Ethanol on Chemically Synthesized Polyaniline Nanothread. *J. Appl. Polym. Sci.* **2006**, *99*, 1848−1853.
(59) Jung, W. K.; Koo, H. C.; Kim, K. W.; Shin, S.; Kim, S. H.; Park, Y. H. Antibacterial Activity and Mechanism of Action of the Silver Ion in Staphylococcus aureus and Escherichia coli. *Appl. Environ. Microbiol.* **2008**, *74*, 2171−2178.